Spin fine-structure reveals bi-exciton geometry in an organic semiconductor

K. M. M Yunusova, S. L. L Bayliss, T. Chanelière, V. Derkach, J. E. E Anthony, Alexei Chepelianskii, L. R. R Weiss

Spin fine-structure reveals bi-exciton geometry in an organic semiconductor

K.M. Yunusova,[1] S. L. Bayliss,[1,2] T. Chanelière,[3,4] V. Derkach,[5]
J. E. Anthony,[6] A.D. Chepelianskii*,[1] and L. R. Weiss*[7]

[1] *LPS, Univ. Paris-Sud, CNRS, UMR 8502, F-91405, Orsay, France*
[2] *Pritzker School of Molecular Engineering, University of Chicago, Chicago, IL, USA*
[3] *Laboratoire Aimé Cotton, CNRS, Univ. Paris-Sud, ENS-Cachan, Université Paris-Saclay, 91405, Orsay, France*
[4] *Univ. Grenoble Alpes, CNRS, Grenoble INP, Institut Néel, 38000 Grenoble, France*
[5] *O. Ya. Usikov Institute for Radiophysics and Electronics of NAS of Ukraine 12, Acad. Proskury st., Kharkov, 61085, Ukraine*
[6] *Department of Chemistry, University of Kentucky, Lexington, KY 40506-0055, USA*
[7] *Cavendish Laboratory, J. J. Thomson Avenue, University of Cambridge, Cambridge CB3 0HE, UK*

In organic semiconductors, bi-exciton states are key intermediates in carrier-multiplication and exciton annihilation. Of particular recent interest is the spin-2 (quintet) bi-exciton. Comprised of two triplet excitons, the bi-exciton can be formed by singlet fission (the formation of two triplet excitons from one singlet state) or by triplet-triplet annihilation (the reverse process). Of interest for photovoltaics and photocatalysis, the wavefunction of these optically dark bi-excitons is difficult to probe and predict. However, the local geometry of the pair-state is imprinted in the fine structure of its spin Hamiltonian. To access the fine structure of the quintet-state we develop and deploy broadband optically detected magnetic resonance ($0-9$ GHz). Here we correlate the experimentally extracted spin structure with the molecular crystal structure to identify the specific molecular pairings on which the bi-exciton state resides.

I. INTRODUCTION

Bi-exciton states are key excited-state species in a range of nano-structured materials from quantum-confined inorganic systems [1–3] to synthetic molecular structures [4–6]. In organic semiconductors the exciton-pair is an intermediate in both the process of singlet fission [7–9] – the formation of a pair of spin-1 (triplet) excitons from an initial spin-0 (singlet) excitation – and its reverse process, triplet-triplet annihilation [10]. While singlet fission is of particular interest for photovoltaics [11–13] where it has been shown to increase efficiencies of solar energy harvesting beyond traditional limits [14, 15], triplet-triplet annihilation enables the up-conversion of light via the conversion of two low-energy triplet excitons to one higher energy singlet excitation [10, 16]. This process is of particular interest for catalysis [17, 18], photovoltaics [16, 19], and bio-imaging [20, 21]. In both fission and annihilation the bi-exciton state mediates the transition between one excited-state and two dissociated excited-states [22–24].

The wavefunction of these transient, intermediate pairs remains challenging to probe. Purely optical characterization of bi-excitons can be ambiguous as their optical signatures typically overlap with those of singly-excited states. By contrast, light-induced spin resonance has played a key role in showing, unexpectedly, that in several molecular systems, singlet fission produces a long-lived, bound spin-2 bi-exciton, termed the quintet state [25–27]. The observation of the quintet state reflects a dominant exchange interaction between the triplets within a pair. This exchange interaction (parametrized by exchange energy J) separates the pure singlet ($S=0$) from the triplet ($S=1$), and quintet ($S=2$) pairings by J and $3J$ respectively [28]. The spin signatures of this strongly coupled state provide an unambiguous marker of the bi-exciton state [26, 28].

Where are such pairs located in a solid-state system with many possible pair configurations? Here the sensitivity to inter-spin distance and orientation of the spin dipole-dipole interaction provides a window into the geometry of the multi-exciton state. Indeed, spin-spin dipolar interactions are used as a ruler for nano-scale distances in widespread applications of spin-labels to biological and synthetic systems [29]. Typically non-native spin-probes are required to take advantage of the dipolar interaction between synthetic radical-bearing ligands attached to biologically relevant structures. Conveniently, the dipolar interactions between the two triplet states in the quintet Hamiltonian provides a native probe of its spatial confinement and orientation [30, 31].

These dipolar interactions are reflected in the fine structure in the quintet (and triplet) spin manifold: the energetic splitting within the spin-manifold even in the absence of a magnetic field. The *zero-field splitting* (ZFS) Hamiltonian in its principal axes takes the form

$$\hat{H}_{zfs}/h = \mathbf{S}^T\cdot\mathbf{D}\cdot\mathbf{S} = D(\hat{S}_z^2 - \frac{1}{3}S(S+1)) + E(\hat{S}_x^2 - \hat{S}_y^2) \quad (1)$$

where $\mathbf{D}$ is the dipolar tensor (D-tensor) and $\mathbf{S}$ is the relevant vector of spin operators (with total spin $S=1,2$ for triplet, quintet states) defined along the principal axes ($\hat{x}$, $\hat{y}$, $\hat{z}$) of the D-tensor. These directions are defined by the symmetry of the spin distribution with the $\hat{z}$-axis defined by the axis of maximum absolute magnitude of dipolar coupling. The strength of the dipolar coupling

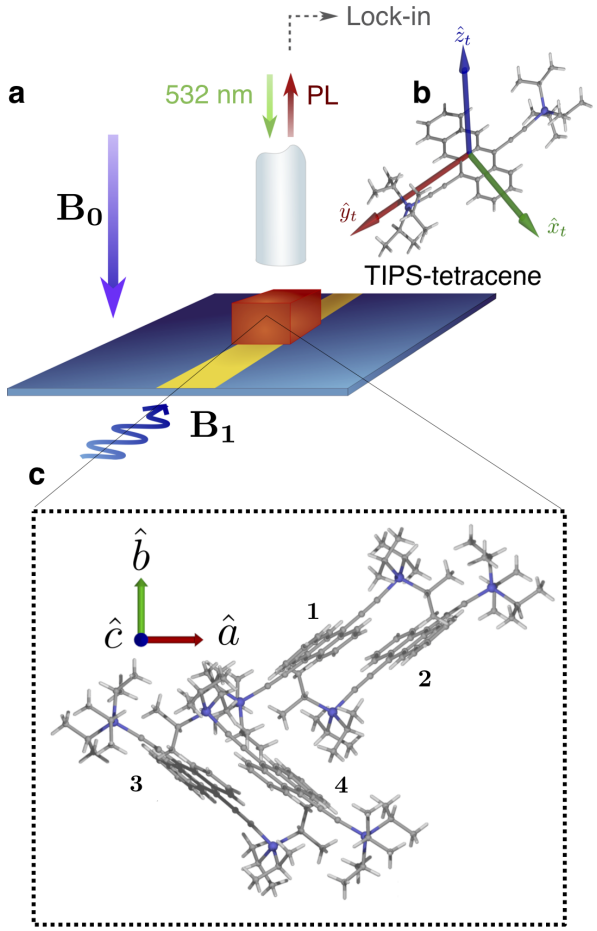

Figure 1. Broadband ODMR of the triplet-pair state. (a) Schematic of the experimental set-up. Crystalline samples of TIPS-tetracene were optically illuminated (532 nm, continuous-wave (CW) excitation) under amplitude-modulated microwave excitation ($\mathbf{B_1}$) using a broadband strip-line ($0-9$ GHz) in liquid helium (4 K). Photoluminescence was collected (via 1 mm core optical fiber) to detect the microwave-induced change in photoluminescence (ODMR) as a function of both microwave frequency and static magnetic field ($\mathbf{B}_0$) with $\mathbf{B}_0 \perp \mathbf{B}_1$. (b) Molecular structure of TIPS-tetracene and corresponding principal axes of the intra-triplet dipolar interaction ($\hat{x}_t, \hat{y}_t, \hat{z}_t$). (c) Solid-state crystal structure of TIPS-tetracene with four rotationally inequivalent molecules per unit cell labelled 1-4 and unit cell axes ($\hat{a}, \hat{b}, \hat{c}$).

parameters (D, E) reflect the degree of confinement and asymmetry of the spin-system as we describe in detail in the next section.

Experimentally these parameters (D, E and $\hat{x}, y, \hat{z}$) can be extracted from magnetic resonance spectra, which can be detected via microwave absorption in a cavity or via spin-dependent electrical or optical transitions. In this work we use optically detected magnetic resonance (ODMR) as shown in Fig. 1a, which combines three key advantages for probing the geometry of the transient bi-exciton state: (1) sensitivity of photoluminescence-detection to the recombination of intermediate states, (2) detection sensitivity from optical (versus microwave) read-out, and (3) the sensitivity to dipolar interactions (on the MHz-GHz scale) of magnetic resonance.

II. THEORY

In this section we establish the relationship between the triplet pair geometry and the resulting measurable $S = 2$ bi-exciton fine structure (D_Q, E_Q and the principal axes $\hat{x}_q, \hat{y}_q, \hat{z}_q$), which we then go on to determine experimentally. Previous measurements of quintet states in various materials have found that $D_Q \sim D_T/3$ [25, 26], yet this relation holds only in the case of co-linear triplet D-tensors and in the absence of dipolar coupling between the excitons, and so acts as an approximate guide to identifying quintet spectra [31].

For triplet excitons in organic semiconductors D_T and E_T are set by the spatially averaged spin-spin interaction of electron and hole, reflecting triplet states localized on a single molecule in the material used here, TIPS-tetracene [32, 33]. As shown in Fig. 1b, the $\hat{z}$-axis of maximal spin-spin coupling is out of the plane of the TIPS-tetracene molecule and the $\hat{x}$- and $\hat{y}$-axes are in the plane of the molecule along the long and short axes.

The $S = 2$ triplet-pair fine-structure depends on the underlying orientation of two such triplets localized on two molecules (labeled here A and B). We assume that each triplet has the same zero-field parameters (D_T, E_T) and differ only in orientation and position. We define the principal axes of the triplet state on molecule A as $(\hat{x}_a, \hat{y}_a, \hat{z}_a)$ and on molecule B as $(\hat{x}_b, \hat{y}_b, \hat{z}_b)$ with the unit vector between them given by $\hat{u}_{ab} = \vec{r}_{ab}/|\vec{r}_{ab}|$. The zero-field Hamiltonian of the pair in the uncoupled basis is then given by

$$\hat{H}^{(1\otimes1)}_{zfs}/h = \sum_{i=a,b} \mathbf{S}_i^T \cdot \mathbf{D}_T^i \cdot \mathbf{S}_i - \Gamma(\hat{u}_{ab}\cdot\mathbf{S}_a)(\hat{u}_{ab}\cdot\mathbf{S}_b) + J\mathbf{S}_a\cdot\mathbf{S}_b \tag{2}$$

where $\Gamma = \frac{3\mu_0\mu_B^2 g^2}{4\pi|\vec{r}_{ab}|^3}$ gives the strength of the dipolar interaction with μ_0 the magnetic permeability of free-space, μ_B the Bohr magneton, g the g-factor, and $|\vec{r}_{ab}|$ the inter-triplet distance. In the limit of strong exchange coupling ($J \gg D_T$) the Hamiltonian is approximately diagonal in the coupled spin-basis defined by the states of pure total spin [28, 34, 35]. Projecting the above Hamiltonian into the $S = 2$ subspace and converting to the coupled basis gives the quintet zero-field Hamiltonian as

$$\hat{H}^{(2)}_{zfs}/h = \mathbf{S}^T \cdot \mathbf{D}_Q \cdot \mathbf{S} \tag{3}$$

where $\mathbf{S} = (\hat{S}_x, \hat{S}_y, \hat{S}_z)$ are the Pauli spin operators for total spin-2. The quintet zero-field tensor $\mathbf{D}_Q$ in terms of the underlying triplet fine structure, inter-triplet distance, and dipolar interaction is given by

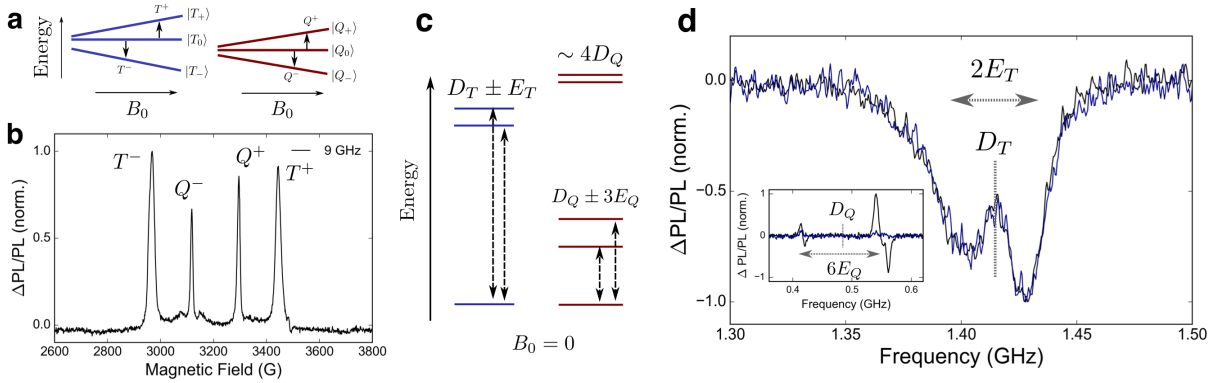

Figure 2. Field-swept and zero-field ODMR of the triplet pair state.
(a) Energy levels of the triplet and quintet $m = 0, \pm 1$ sub-levels as a function of field with transitions at 9 GHz marked with arrows to correspond to experimentally observed transitions in (b). (b) ODMR spectrum at 9 GHz showing inner quintet transitions ($Q^{\pm}$) and the outer triplet transitions ($T^{\pm}$). (c) Energy level diagram of triplet and quintet zero-field spin sub-levels. (d) Zero-field ODMR spectrum where the triplet transitions are split by the zero-field E_T-parameter and with centre frequency set by the D_T-parameter. Inset: Low frequency quintet transitions marked with corresponding zero-field splitting parameters (D_Q, E_Q) of the quintet pair-state.

$$\mathbf{D}_Q = \frac{D_T}{6}\left(\sum_{i=a,b} \hat{z}_i \hat{z}_i^T - \frac{2}{3}\hat{I}_3\right) \qquad (4)$$
$$+\frac{E_T}{6}\sum_{i=a,b}\left(\hat{x}_i\hat{x}_i^T - \hat{y}_i\hat{y}_i^T\right) - \frac{\Gamma}{3}\left(\hat{u}_{ab}\hat{u}_{ab}^T - \frac{1}{3}\hat{I}_3\right)$$

where the full derivation is given in the Supporting Information (Appendix A). The eigenvalues of $\mathbf{D}_Q$ are ordered $|D_y| < |D_x| < |D_z|$, which gives $D_Q = \frac{3}{2}D_z$, $E_Q = \frac{1}{2}(D_y - D_x)$, and the principal axes $\hat{x}_q, \hat{y}_q, \hat{z}_q$ (the eigenvectors of $\mathbf{D}_Q$). In the following sections we will apply this framework to link the measured values and orientation of the D-tensors of the triplet and quintet states to their localization in the crystal structure of TIPS-tetracene.

III. FINE STRUCTURE TENSOR PARAMETERS OF THE QUINTET STATE

TIPS-tetracene is a solution-processable singlet fission material of interest for its high singlet fission efficiency [36, 37]. Structured with side-chain modification of the canonical fission molecule, tetracene, as shown in Fig. 1b, TIPS-tetracene crystallizes with a distinct molecular packing shown in Fig. 1c. The unit cell contains four orientationally inequivalent molecules yielding six possible nearest-neighbor pair sites within a unit cell in addition to non-crystalline defect sites. Both bi-excitons and free triplet excitons have been identified in this material with transient electron spin resonance, but the nature of the local site housing the bound pair remains a key question. The theoretical framework above demonstrates how the parameters of the quintet fine structure (its principal values D_Q, E_Q and the orientation of the principal axes $\hat{x}_q, \hat{y}_q, \hat{z}_q$) are specific to the geometry of the underlying triplet pair and so each distinct potential pair site can be identified by its unique fine structure parameters in a single crystal. (Note that these parameters are calculated explicitly from the crystal structure for each of the six possible pair states and reported in Section V).

With this motivation we use a macroscopic crystal (∼mm-scale single-crystalline domain) and measure the principal values of the D-tensors of the triplet and quintet states using broadband zero-field ODMR and then apply a magnetic field to find the orientation of their principal axes in the laboratory frame in Section IV. The experimental setup is shown in Fig. 1a and includes 532 nm continuous-wave (CW) light excitation, microwave radiation ($\mathbf{B}_1$) with variable frequency delivered by a broadband copper strip-line and a static magnetic field ($\mathbf{B}_0$). The ODMR signal is measured by lock-in detection of microwave-induced changes in photoluminescence (see the Methods section for further details).

We first perform standard fixed-frequency (9 GHz) field-swept ODMR to confirm that, in agreement with previous measurements using transient electron spin resonance, we observe two pairs of spin-transitions consistent with the $\Delta m = \pm 1$ transitions of the $S = 1$ triplet exciton ($T^{\pm}$) and the $\Delta m = \pm 1$ transitions of the $S = 2$ quintet state ($Q^{\pm}$), as shown in Fig. 2b [26, 27]. The corresponding energy-level diagrams and transitions fields are shown in Fig. 2a.

These observed high-field transitions are correlated with zero-field transitions (magnetic field strength $B_0 = 0$, Fig. 2c,d), measured for the first time here. These zero-field spectra allow us to extract the zero-field splitting parameters for the triplet and quintet states directly.

In the absence of a magnetic field, the energy eigenstates of triplets and quintets are determined by their spin-spin dipolar interactions. The energy eigenstates are given by the $B_0 = 0$ spin-eigenstates. Microwave transitions at zero-field are determined by the energy-splitting between these zero-field states. As shown in the theoretical sketch in Fig. 2c, the triplet energy levels are separated in energy by $|D_T|$ and further split by $|2E_T|$ between the two upper eigenstates, where D_T and E_T are the zero-field splitting parameters for the triplet. Zero-field ODMR resonances therefore occur at microwave frequencies $\nu = D_T \pm E_T$.

The quintet eigenstates in zero-field are likewise defined by the eigenstates of the quintet fine-structure tensor. As shown in Fig. 2c, the three lowest quintet levels are split by $|D_Q|$ from the ground state to the first two states with a further splitting of $|6E_Q|$ between those two upper levels. This leads to ODMR transition frequencies at $\nu = D_Q \pm 3E_Q$. Note that the previously reported D-parameters for TIPS-tetracene are $D_T \sim 1.4$ GHz and $D_Q \sim D_T/3$ [26, 33]. However previous experiments did not determine E-parameters and molecular frame orientations which, as we will show, are needed to identify the contribution of triplet dipole-dipole interaction to the quintet fine structure tensor.

The magnetic resonance spectra of triplets and bi-excitons can be distinguished in ODMR due to the difference in lifetime of the two species [26, 33]. The microwave amplitude modulation frequency (137 Hz) is chosen to correspond with the inverse lifetime of the longer-lived species (triplets), which then appear with equal amplitude on the in-phase (X-channel) and out-of-phase (Y-channel) lock-in channels. The signal from shorter lived bi-excitons appears only on the X-channel and can be isolated by subtracting X and Y channels. The zero-field X- and Y-channel ODMR spectra are plotted in Fig. 2d in black (X-channel) and blue (Y-channel). The transitions on the Y-channel are consistent with triplets with $|D_T| = 1.4$ GHz and $|E_T| = 14$ MHz (Fig. 2d). Transitions in the frequency region expected for the quintet only appear on the X-channel and give $|D_Q| = 477$ MHz and $|E_Q| = 22$ (Fig. 2d inset). The sign of D_T was determined in Ref. [26] to be positive, which in turn determines E_T to be negative. The resolution of the splitting afforded by this technique allows extraction of E_Q and E_T, highlighting the sensitivity of the zero-field approach. The measurement of the E-parameters here is made possible by the reduced linewidths observed at zero-field relative to previous measurements under non-zero magnetic field.

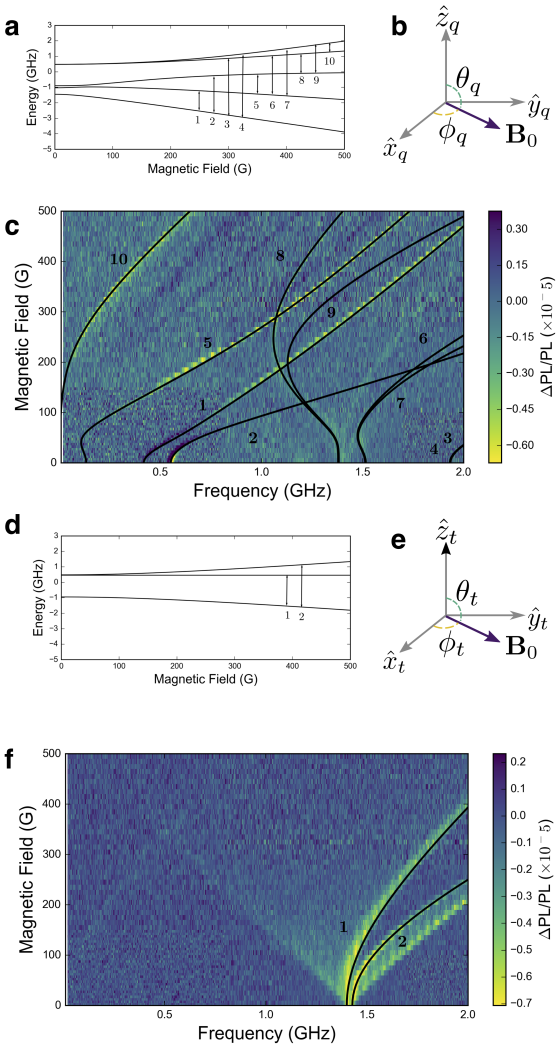

Figure 3. Fine-structure tensor from from broadband ODMR. (a,d) Energy level diagram for the quintet (a) and triplet (d) states as a function of magnetic field. Arrows indicate potential transitions, corresponding to lines on Fig. 3c and 3f respectively. (b,e) Schematic representation of the orientation of **B** in the quintet (b) and triplet (e) fine-structure axes. (c) ODMR transitions associated with the quintet state with overlay of simulated transitions. Signal has been isolated by subtracting a scaled out-of-phase (Y)-channel signal from the in-phase signal to remove triplet contributions. Black lines show simulations given for $\theta_q = 90°$ and $\phi_q = 30°$ with an uncertainty of $\pm 5°$. (f) Y-channel (out-of-phase) ODMR map of ODMR transitions attributed to the triplet state with overlay of calculated transitions for the triplet state in black with $\theta_t = 90°$.

IV. EXTRACTION OF BI-EXCITON FINE STRUCTURE ORIENTATION

Having extracted the principal components of the triplet and quintet fine-structure tensors at zero-field, we now map the resonant frequencies as a function of magnetic field to determine the corresponding orientations of the principal axes. The experimental ODMR maps for quintet and triplet states are shown in Fig. 3c,f (separated by lock-in detection phase as described in the previous section).

The orientation of the quintet fine-structure axes in the lab frame is obtained by fitting these maps with the

spin transitions predicted by the fine structure parameters determined at zero-field (see Sec. III) with the orientation as input. The polar angle θ and azimuthal angle ϕ parametrize the orientation of the principal axes relative to the magnetic field in the laboratory frame as shown in Fig. 3b,e. There are 10 possible transitions between the five quintet spin sub-levels (Fig. 3a), which are overlaid on the quintet ODMR map (Fig. 3c). It should be noted that the visibility of transitions depends on populations and selection rules, and transitions 3,4,9, and 6 are not observed experimentally. The observed resonances cannot be fit by a spin-1 state, which further confirms the assignment (see SI). The quintet state is oriented with fixed $\theta_q = 90 \pm 5°$ between $\hat{z}_q$ and $\mathbf{B}_0$ and $\phi_q = 30 \pm 5°$ between $\hat{x}_q$ and $\mathbf{B}_0$.

The evolution of the ~ 1.4 GHz zero-field transitions with field, shown in Fig. 3f are consistent with $\theta_t, = 0°$ and $\theta_t = 90°$ with the latter perpendicular component more prominent (calculated transitions for $\theta_t = 90°$ are plotted in black) and the $\theta_t = 0°$ consistent with the presence of a weak powder background. The dominant $\theta_t = 90°$ triplet orientation correlates with the high-field spectrum (Fig. 2b): triplet peaks are separated by $\Delta B_0 \sim D/g\mu_B$, which occurs when $\theta_t \sim 90°$, whereas no peaks are observed for $\theta_t \sim 0$ (separation $\Delta B_0 \sim 2D/g\mu_B$) . [Note that ϕ_t could not be extracted reliably as $E_T \ll D_T$, and this parameter was not required for subsequent analysis because the triplet states are nearly axially symmetric (i.e., as $E_T \approx 0$, E_Q and D_Q do not depend significantly on the relative orientation of $\hat{x}_t$ and $\hat{y}_t$).] As the D-tensor values and orientations in the laboratory frame are obtained from a bulk crystalline sample, we can now compare them with the theoretically predicted D-tensors in the TIPS-tetracene crystal structure.

V. PAIR SITES IN THE TIPS-TETRACENE CRYSTAL STRUCTURE

We now compare the experimental observations to the quintet fine-structure theoretically predicted in the TIPS-tetracene crystal structure. As shown in Fig. 1c, in the TIPS-tetracene unit-cell molecules are packed with two approximately parallel dimers each rotated with respect to the other by $\sim 90°$ about the $\hat{c}$ axis. There are six potential nearest-neighbor dimer configurations and for each we can calculate the expected D_Q, E_Q parameters using Eq. (4), the molecular triplet axes shown in Fig. 1b and the intermolecular distances extracted from the crystal structure determined by X-ray diffraction [38]. These values are summarized in Table I where we have taken nearest-neighbor dimer configurations. (We note that we have taken a point-dipole approximation for each triplet localized at the center of each molecule in the pair which is likely the main source of error in the predicted fine structure parameters.)

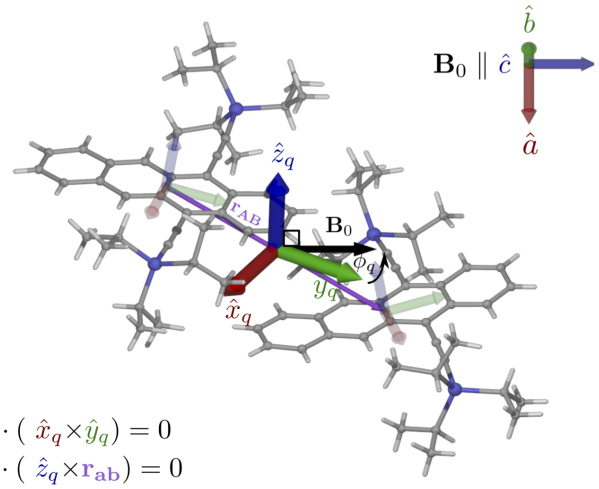

Figure 4. Local geometry of the quintet fine-structure tensor in the TIPS-tetracene crystal with an angle of $\theta_q = 91.6°$ and $\phi_q = 30.6°$, where the crystal is oriented with $\mathbf{B}_0 \parallel \hat{c}$ with two co-planar triads of vectors, $(\hat{x}_q, \hat{y}_q, \mathbf{B}_0)$ and $(\hat{z}_q, \mathbf{r}_{ab}, \mathbf{B}_0)$.

	$\lvert D_Q \rvert$ (MHz)	$\lvert E_Q \rvert$ (MHz)	θ_q (deg.)	ϕ_q (deg.)	r_{ab} (Å)
$TT_{1,2}$	474.0	22.5	91.6°	30.6°	10.0
$TT_{1,3}$	227.5	72.4	13.5°	77.8°	10.5
$TT_{1,4}$	250.4	42.7	15.5°	84.7°	9.7
$TT_{2,3}$	234.8	62.0	13.8°	90.8°	15.7
$TT_{2,4}$	245.5	69.7	11.0°	78.9°	17.7
$TT_{3,4}$	474.0	22.5	88.4°	30.6°	10.0
Obs.	477 ± 1	22 ± 1	$90.0 \pm 5°$	$30 \pm 5°$	-

Table I. Predicted fine structure parameters from distances in TIPS-tetracene crystal structure with $\lvert D_T \rvert = 1414$ MHz and $\lvert E_T \rvert = 14$ MHz from the measured zero-field values with angles given between $\mathbf{B}_0$ and $\hat{z}_q$ (θ_q) and $\hat{x}_q$ (ϕ_q) for $\mathbf{B}_0 \parallel \hat{c}$. The final row shows the corresponding experimental observations, consistent with the predicted values of $TT_{1,2}$ and $TT_{3,4}$, highlighted in blue.

The observed quintet and triplet signatures and extracted angles of $\theta_q \sim 90°$ and $\phi_q \sim 30°$ are consistent with exchange-coupled triplets localized on dimers 1,2 and 3,4 (highlighted in blue in Table I) where molecules in the unit cell are labeled $1-4$ in Fig. 1c and the calculated angles are for $\mathbf{B}_0 \parallel \hat{c}$ as this orientation is consistent with known crystal facets, both the quintet and triplet transition maps, and the 9 GHz field-swept spectrum presented in Fig. 1c (see SI). Interestingly, these dimer configurations correspond to the most closely π-stacked dimers in the crystal suggesting that this geometry is favorable for binding of the multi-exciton state. The extracted local quintet fine structure is visualized in Fig. 4 where the full quintet and triplet dipolar interactions are shown with respect to the magnetic field in the lab frame and crystallographic axes, summarizing

the local structure of quintet and triplet states in TIPS-tetracene and their relation to intermolecular geometry.

VI. CONCLUSIONS

We have developed the theoretical and experimental approaches to connect inter-molecular structure and bi-exciton geometry. In the context of organic semiconductors, understanding this connection presents a path toward molecular engineering of bi-excitons. We find that the triplet pair is localized on the closest π-stacked dimers of the crystal structure. As the fine structure is consistent with minimal modification from the ground-state crystal structure, these results suggest that geometric reorganization is negligible in the quintet bi-exciton excited-state. This description of the geometry of the triplet pair therefore sets the foundation for orientation-selective, all-optical experiments where time-resolved measurements would allow investigation of the transient localization and molecular reorganization of the pair-state.

Further, we have shown that the energy-level structure, determined by the inter and intra-triplet dipolar interactions, is highly sensitive to the underlying molecular structure. This sensitivity of the effective spin Hamiltonian to intermolecular geometry further opens up opportunities to tune spin parameters via crystal structure engineering of spin-based organic devices. Tuning spin energy levels and zero-field interactions is critical in spin-based applications, for example in tuning the amplification frequency in the newly emerging class of organic molecular masers [39, 40] or in minimizing spin relaxation and dephasing [41, 42]. Dipolar spin interactions thereby provide a route toward engineering the spin level-structure in organic materials in future spin-based quantum technologies.

[1] Bryant, G. W. Biexciton binding in quantum boxes. *Physical Review B* **41**, 1243 (1990).

[2] Chen, G. *et al.* Biexciton quantum coherence in a single quantum dot. *Physical review letters* **88**, 117901 (2002).

[3] Hu, Y. *et al.* Biexcitons in semiconductor quantum dots. *Physical review letters* **64**, 1805 (1990).

[4] Baldo, M. A., Adachi, C. & Forrest, S. R. Transient analysis of organic electrophosphorescence. ii. transient analysis of triplet-triplet annihilation. *Physical Review B* **62**, 10967 (2000).

[5] Klimov, V., McBranch, D., Barashkov, N. & Ferraris, J. Biexcitons in π-conjugated oligomers: Intensity-dependent femtosecond transient-absorption study. *Physical Review B* **58**, 7654 (1998).

[6] Masui, K., Nakanotani, H. & Adachi, C. Analysis of exciton annihilation in high-efficiency sky-blue organic light-emitting diodes with thermally activated delayed fluorescence. *Organic Electronics* **14**, 2721–2726 (2013).

[7] Smith, M. B. & Michl, J. Singlet fission. *Chemical reviews* **110**, 6891–6936 (2010).

[8] Singh, S., Jones, W., Siebrand, W., Stoicheff, B. & Schneider, W. Laser generation of excitons and fluorescence in anthracene crystals. *The Journal of Chemical Physics* **42**, 330–342 (1965).

[9] Swenberg, C. & Stacy, W. Bimolecular radiationless transitions in crystalline tetracene. *Chemical Physics Letters* **2**, 327–328 (1968).

[10] Singh-Rachford, T. N. & Castellano, F. N. Photon upconversion based on sensitized triplet–triplet annihilation. *Coordination Chemistry Reviews* **254**, 2560–2573 (2010).

[11] Rao, A. & Friend, R. H. Harnessing singlet exciton fission to break the shockley–queisser limit. *Nature reviews materials* **2**, 17063 (2017).

[12] Hanna, M. & Nozik, A. Solar conversion efficiency of photovoltaic and photoelectrolysis cells with carrier multiplication absorbers. *Journal of Applied Physics* **100**, 074510 (2006).

[13] Tayebjee, M. J., Gray-Weale, A. A. & Schmidt, T. W. Thermodynamic limit of exciton fission solar cell efficiency. *The Journal of Physical Chemistry Letters* **3**, 2749–2754 (2012).

[14] Einzinger, M. *et al.* Sensitization of silicon by singlet exciton fission in tetracene. *Nature* **571**, 90 (2019).

[15] Congreve, D. N. *et al.* External quantum efficiency above 100% in a singlet-exciton-fission–based organic photovoltaic cell. *Science* **340**, 334–337 (2013).

[16] Cheng, Y. Y. *et al.* On the efficiency limit of triplet–triplet annihilation for photochemical upconversion. *Physical Chemistry Chemical Physics* **12**, 66–71 (2010).

[17] Ravetz, B. D. *et al.* Photoredox catalysis using infrared light via triplet fusion upconversion. *Nature* **565**, 343 (2019).

[18] Khnayzer, R. S. *et al.* Upconversion-powered photoelectrochemistry. *Chemical Communications* **48**, 209–211 (2012).

[19] Gray, V., Dzebo, D., Abrahamsson, M., Albinsson, B. & Moth-Poulsen, K. Triplet–triplet annihilation photon-upconversion: towards solar energy applications. *Physical Chemistry Chemical Physics* **16**, 10345–10352 (2014).

[20] Liu, Q., Yang, T., Feng, W. & Li, F. Blue-emissive upconversion nanoparticles for low-power-excited bioimaging in vivo. *Journal of the American Chemical Society* **134**, 5390–5397 (2012).

[21] Liu, Q. *et al.* Highly photostable near-ir-excitation upconversion nanocapsules based on triplet–triplet annihilation for in vivo bioimaging application. *ACS applied materials & interfaces* **10**, 9883–9888 (2018).

[22] Burdett, J. J. & Bardeen, C. J. Quantum beats in crystalline tetracene delayed fluorescence due to triplet pair coherences produced by direct singlet fission. *Journal of the American Chemical Society* **134**, 8597–8607 (2012).

[23] Merrifield, R. Theory of magnetic field effects on the mutual annihilation of triplet excitons. *The Journal of Chemical Physics* **48**, 4318–4319 (1968).

[24] Zimmerman, P. M., Zhang, Z. & Musgrave, C. B. Singlet fission in pentacene through multi-exciton quantum states. *Nature chemistry* **2**, 648 (2010).

[25] Tayebjee, M. J. *et al.* Quintet multiexciton dynamics in singlet fission. *Nature Physics* **13**, 182 (2017).

[26] Weiss, L. R. *et al.* Strongly exchange-coupled triplet pairs

in an organic semiconductor. *Nature Physics* **13**, 176 (2017).
[27] Lubert-Perquel, D. *et al.* Multiple quintets via singlet fission in ordered films at room temperature. *Nature Communications* **9**, 4222 (2018).
[28] Bayliss, S. L. *et al.* Site-selective measurement of coupled spin pairs in an organic semiconductor. *Proceedings of the National Academy of Sciences* **115**, 5077–5082 (2018).
[29] Berliner, L. J. & Reuben, J. *Spin labeling: theory and applications*, vol. 8 (Springer Science & Business Media, 2012).
[30] Weil, J. A. & Bolton, J. R. *Electron paramagnetic resonance: elementary theory and practical applications* (John Wiley & Sons, 2007).
[31] Benk, H. & Sixl, H. Theory of two coupled triplet states: Application to bicarbene structures. *Molecular Physics* **42**, 779–801 (1981).
[32] Bayliss, S. L. *et al.* Localization length scales of triplet excitons in singlet fission materials. *Physical Review B* **92**, 115432 (2015).
[33] Bayliss, S. L. *et al.* Geminate and nongeminate recombination of triplet excitons formed by singlet fission. *Physical review letters* **112**, 238701 (2014).
[34] Bayliss, S. L. *et al.* Spin signatures of exchange-coupled triplet pairs formed by singlet fission. *Physical Review B* **94**, 045204 (2016).
[35] Yago, T., Ishikawa, K., Katoh, R. & Wakasa, M. Magnetic field effects on triplet pair generated by singlet fission in an organic crystal: application of radical pair model to triplet pair. *The Journal of Physical Chemistry C* **120**, 27858–27870 (2016).
[36] Stern, H. L. *et al.* Vibronically coherent ultrafast triplet-pair formation and subsequent thermally activated dissociation control efficient endothermic singlet fission. *Nature chemistry* **9**, 1205 (2017).
[37] Stern, H. L. *et al.* Identification of a triplet pair intermediate in singlet exciton fission in solution. *Proceedings of the National Academy of Sciences* **112**, 7656–7661 (2015).
[38] Eaton, D., Parkin, S. & Anthony, J. Ccdc 962667: Experimental crystal structure determination. *CCCDC* (2013).
[39] Oxborrow, M., Breeze, J. D. & Alford, N. M. Room-temperature solid-state maser. *Nature* **488**, 353 (2012).
[40] Bogatko, S. *et al.* Molecular design of a room-temperature maser. *The Journal of Physical Chemistry C* **120**, 8251–8260 (2016).
[41] Solomon, I. Relaxation processes in a system of two spins. *Physical Review* **99**, 559 (1955).
[42] Shiddiq, M. *et al.* Enhancing coherence in molecular spin qubits via atomic clock transitions. *Nature* **531**, 348 (2016).

Acknowledgments We are thankful for insightful discussions with H. Bouchiat and R.H. Friend and acknowledge support from ANR SPINEX and Labex ANR-10-LABX-0039-PALM. L.R. Weiss acknowledges support from the Clare College Junior Research Fellowship.

Author Contributions The data were measured and analyzed by K.M.Y., L.R.W., and A.D.C. J.E.A. provided materials. All authors contributed to planning the experiment, discussions and the preparation of the manuscript.

Author Information The authors declare no competing financial interests. Correspondence should be addressed to A.D.C. (chepelianskii@lps.u-psud.fr) and L.R.W (lrweiss@uchicago.edu).

Methods Optically detected magnetic resonance is performed 532 nm CW laser illumination via 1 mm-diameter optical fiber (Fig. 1a) in liquid helium at 4 K. An amplitude modulated microwave field ($\mathbf{B}_1$) in a frequency range $0 - 9$ GHz was applied using a broadband copper stripline. The sample holder was fixed inside a superconducting solenoid. Photoluminescence was collected (via the same optical fiber and avalanche photodiode) to detect the microwave-induced change in photoluminescence (ODMR) as a function of both microwave frequency and static magnetic field ($\mathbf{B}_0$) with $\mathbf{B}_0 \perp \mathbf{B}_1$.